Electromagnetic Interference Shielding Performance Enhancement of Stretchable Transparent Conducting Silver Nanowire Networks with Graphene Encapsulation

Siyi Yan
Northeast Normal University
Peng Li (lip032@nenu.edu.cn)
Northeast Normal University https://orcid.org/0000-0002-0933-2592
Zhongshi Ju
Northeast Normal University
He Chen
Northeast Normal University
Jiangang Ma
Northeast Normal University

Research Article

Keywords: stretchable transparent electrodes, graphene, silver nanowires, electromagnetic interference shielding

Posted Date: March 1st, 2021

DOI: https://doi.org/10.21203/rs.3.rs-260780/v1

Abstract

Silver nanowire (AgNW) networks are promising transparent conducting materials for electromagnetic interference (EMI) shielding and diverse optoelectronic devices. However, the poor contact between adjacent AgNWs leads to low electrical conductivity and weak mechanical stability of AgNW networks, which are limiting the practical application of these electronics. Here we report an efficient strategy to improve the overall performance of AgNW networks, in which the AgNW networks are sandwiched between two layers of graphene films. The graphene films improve the contact of overlapped AgNWs and bridge the discrete AgNWs, and thus increase the conductivity of graphene/AgNWs/graphene (GAG) films. Microwave permittivity measurements together with mechanism analyses reveal that the graphene films can enhance the EMI shielding effectiveness of AgNW networks through offering extra conduction loss, multiple dielectric polarization centers and multi-reflection processes. As a result, the GAG film with an average transmittance of 88% exhibits a sheet resistance lower than 15 Ω sq^{-1} and an EMI shielding effectiveness of 31 dB (in the frequency range of 8.2–12.4 GHz) after repeated stretching and release at a strain of 40%. Such a total performance is superior to that of most of as-reported transparent conductors. The GAG films therefore show application potential in the age of Internet of Things that electromagnetic radiation pollutions are everywhere.

Introduction

Transparent conducting materials are widely used as electrodes in diverse optoelectronic devices such as solar cells, flat-panel displays and touch screens, and also play a key role in electromagnetic interference (EMI) shielding application [1–4]. In the age of Internet of Things, increasing military and civilian communication equipments that inevitably emit innumerous electromagnetic waves are used. Electromagnetic radiation has become one of the most serious pollutions that not only causes malfunction of electronic devices, but also is harmful for human body. Therefore, there has been a fast growth in the demand of EMI shielding materials.

Degenerately doped wide band gap semiconductors with forbidden band width higher than the photon energy of visible light, e.g., tin doped indium oxide (ITO), is currently dominating the transparent conducting and EMI shielding material market. However, the fragile ceramic nature of ITO severely limits its application in the wearable electronics which are usually deformable and conformable with curved surfaces. Silver nanowires (AgNWs), graphene and their hybrids are promising candidates to replace the traditional metal oxide semiconductors as alternative flexible transparent conducting materials in the recent years [5–15]. Among them, one-dimensional (1D) AgNWs possess the highest intrinsic conductivity however suffer from low optoelectronic performance due to poor connection of overlapped AgNWs. Two-dimensional (2D) graphene film has mobility as high as 10^4 cm^2 V^{-1} s^{-1} and only absorbs 2.3% of visible light [10], but defects such as ripples and cracks limit the electrical conductivity of graphene. The hybrids of 1D AgNWs and 2D graphene possess good optoelectronic properties and stability because the two components can complement with each other [16].

The encapsulation of AgNW networks with graphene films has many other synergistic effects. Elaborately constructed graphene/AgNWs heterogeneous structures tend to induce interesting physical phenomena under external stimuli like tensile stress or microwave irradiation owing to the configuration difference between AgNWs and graphene in terms of carrier concentration, Young's modulus, dielectric characteristics [17–20]. A pioneering work has demonstrated that the graphene can improve the optical sintering efficiency of a xenon flash lamp by controlling optical transparency and light absorbing yield in stacked graphene/AgNWs electrodes, thereby facilitating the fusion at contacts of AgNWs [21]. Our very recent work finds that the reduced graphene oxide-shells can improve the current carrying capacity of AgNW-cores by suppressing the electromigration of surface silver atoms [22]. However, few attentions have been devoted to the graphene/AgNWs hybrid films to full fill the promise of these materials in EMI shielding application as far as we know [23].

This work investigates the electrical, optical, mechanical and electromagnetic properties of sandwich-structured graphene/AgNWs/graphene (GAG) films. The encapsulation of AgNWs with 2D graphene films reduces the total transmittance by 5%, but lowers the sheet resistance by 3 times due to the improvement in the contact quality of AgNWs. The top and bottom layer 2D graphene film can fracture at different positions to adapt to the deformation of AgNW networks once the GAG films are stretched. The bilayer graphene offers multiple reflection and dielectric polarization processes for the attenuation of incident electromagnetic waves. These findings provide physical insights for in-depth understanding the good EMI shielding performance of the stretchable transparent GAG films.

Experimental Section

Fabrication of GAG films

The polydimethylsiloxane (PDMS) was purchased from Dow Corning Co., Ltd., USA (Sylgard 184). PDMS substrates were prepared by mixing the two “base” and the “curing agent” at a ratio of 10:1 and then keeping the mixture at 70 °C for 2 h. The AgNW solutions (1 mg/ml) were purchased from XFNANO Tech. Co., Ltd., China. The monolayer graphene films grown on the copper foils were prepared by chemical vapor deposition (6Carbon Tech. Co., Ltd., China). The GAG films were fabricated by transferring a monolayer graphene onto the PDMS substrate, spin-coating the AgNWs, and subsequent transferring another layer of graphene. Briefly, the wet chemical transfer process of graphene includes the following steps: spinning a thin layer of polymethylmethacrylate (PMMA) on the graphene surface, etching the bottom layer copper foil with $FeCl_3$ solution, transferring the PMMA/graphene to the target substrate and dissolving the PMMA with acetone [11].

Characterizations and Tests

The surface morphologies of GAG films were characterized by scanning electron microscopy (SEM, FEI QUANTA FEG 250) and atomic force microscopy (AFM, Bruker). The Raman (Horiba) spectra were taken with a 488 nm excitation source. The transmission spectra were measured with a Hitachi UH4150

spectrometer. Kelvin probe force microscopy (KPFM, INNOVA INSP-3) was used to measure the work functions. The sheet resistance were measured with a four-probe system (RTS-9). The tensile experiments were carried out with a home-made setup. The S parameters were recorded with a vector network analyzer (Keysight N5222B PNA).

Results And Discussion

As shown in Fig. 1a, the preparation of GAG film started from transferring a monolayer graphene onto the surface of PDMS substrate. Then the AgNWs were spin-coated and the areal density of AgNWs were controlled by adjusting the number of cycles of spin-coating. Finally, the preparation of GAG film ended up with transferring another layer of graphene. Figure 1b shows the Raman spectrum of GAG film. Three prominent peaks located at wavenumbers of 1350, 1580 and 2630 cm^{-1} are observed, which can be indexed to the D, G and 2D vibration bands of graphene, respectively [24]. The G band is related to phonons of the doubly degenerated zone center E_{2g} mode at the Γ point, and the 2D band associates with two phonons having opposite momentum in the highest optical branch near the K point of the Brillouin zone [15]. The intensity ratio of 2D band to that of G band ($I_{2D/G}$) is widely used as probe to identify the layer number of graphene. As shown in Fig. 1b, the $I_{2D/G}$ of GAG film is in the range of 0.25–0.5, indicating that the number of layers is 2–3 [10]. As $I_{2D/G}$ is also sensitive to the doping states of graphene by electrons or holes, the low $I_{2D/G}$ is likely to be caused by the direct charge transfer between AgNWs and graphene [11]. The AgNWs with high carrier concentration can give electron and lead the Fermi level of graphene to move up, which may cause the intensity reduction of 2D band. The D-band verifies the existence of defects such as wrinkles, folds and vacancies, which may be introduced during the transfer process.

The surface morphologies of GAG films were characterized by SEM and AFM. The SEM image in Fig. 1c illustrates the uniform distribution of AgNWs. Compared with the pure AgNWs which often exhibit high contrast to the insulating substrate, the SEM image of the GAG film is relatively hazy. The static image statistics of more than one hundred of AgNWs shows that the average diameter and length of AgNWs is 25 nm and 30 μm, respectively. The large length to diameter ratio (> 1000) is beneficial for the formation of continuous AgNW networks. In Fig. 1d, the AFM images show that both the surface roughness and the junction height of the GAG are low, indicating that the connection quality of AgNWs is improved by coating graphene. That is reasonable because the wet transfer process of graphene can induce capillary force between overlapped AgNWs due to solvent evaporation and compact the AgNWs together [18].

The optical and electrical properties of the AgNW networks and the GAG films are compared at different AgNW areal densities. As shown in Fig. 2a, the sheet resistance decreases rapidly with the transmittance decreasing. The GAG films exhibit much lower sheet resistance than the AgNW networks while their transmittances are similar. For example, at a transmittance of 85%, the sheet resistance of GAG films is about a quarter of AgNW networks. This reduction in sheet resistance should, if taken for granted, be attributed to the parallel connection of the graphene films and the AgNW network. However, the

experimentally measured sheet resistance is lower than the value calculated by simply assuming such parallel connection. Further characterizations and analyses point out that the AgNWs and the graphene may improve their conductances complementarily instead of providing independent pathways for electrons. First, the AgNWs sandwiched between graphene films are better connected. Thus, the sheet resistance should be much lower due to the decline in junction resistance [25]. Second, our Kelvin probe force microscopy data confirm that electron transfer from AgNWs to graphene could happen because the measured work function of graphene (4.5 eV) is higher than that of AgNWs (4.4 eV). The doping process can improve the electron concentration and enhance the conductivity of graphene. Third, the graphene can assist the connection of isolated AgNWs to decrease discontinuities by providing extra electrical paths (see insets of Fig. 2a). This explanation consists with previous result showing that the graphene can lower the percolation threshold of AgNW networks [26].

Figure 2b plots the transmission spectra of the bilayer graphene film and the GAG films with different initial AgNW densities. The bilayer graphene film exhibits a transmittance higher than 95% throughout the visible spectrum. This high transmittance makes it possible to reduce the total sheet resistance with small transparency loss. Furthermore, the bridge effect of graphene films allows for the improvement of the overall transmittance of GAG films by decreasing the AgNW areal densities without obviously deteriorating conductivity. For example, the transmittance of GAG films can increase from 80.2 to 90.6% with the sheet resistance remaining lower than 20 Ω sq^{-1}. As ideal transparent conductive materials should have high transmittance and low sheet resistance simultaneously, the figure of merit (FoM), defined as FoM = T^{10}/Rs, is employed to evaluate the optoelectronic performance, where T is the transmittance at 550 nm and Rs represents the sheet resistance [27]. The graphene GAG films exhibit two times higher FoMs than AgNW networks, which suggests a better trade-off relationship between T and Rs. Furthermore, the FoM of GAG films is better than that of the ITO films [14].

Apart from the optoelectronic performance, the impacts of graphene on the mechanical stability of AgNWs were also investigated. We evaluate the change of $\Delta R/R_0$ with stretching strains using a homemade setup [28], where R_0 is the original resistance and ΔR is the relative resistance change ($R - R_0$), respectively. As shown in Fig. 2c, $\Delta R/R_0$ of the AgNW networks displays much faster increase rate than that of the GAG films. The $\Delta R/R_0$ of AgNW networks is 0.4 and 0.9 at the strain of 30 and 40% respectively, whereas the resistance of GAG films exhibits slightly increase at the strain smaller than 40%. Figure 2d shows the stretching-releasing cycle dependent resistance at 40% strain. The resistance of GAG films is unchanged and that of AgNW networks shows an obviously ever-increasing trend. Unlike the AgNW networks whose maximum resistance severely fluctuate during repeated stretching-release, both the starting and ending resistances of the GAG film approach to their initial values.

The difference in mechanical stability between the AgNW networks and the GAG films is discussed based on their structural features (insets in Fig. 2c). It is known that the single-crystal AgNWs have much high yield strength due to internal twin boundary-free nature. Thus, the bare AgNWs tend to accommodate the external tensile stress by sliding toward the stretching direction instead of producing plastic deformation.

Maintaining good AgNW junctions is therefore the key to prevent the electrical resistance rise. Owing to the resistance forces residing in the AgNWs/substrate interface, many AgNWs may be unable to recover to their initial positions and then should lose contact with other AgNWs once the tensile strain is released. These dangling discrete AgNWs block the visible light without participating in conducting paths. In contrast, the upper layer graphene can suppress the AgNWs from separation, and thus the GAG films adapt to strain by reversible changing the AgNW network shapes [27], e.g., from rectangle to diamond, without interrupting the junctions. Furthermore, the graphene with high Young's modulus is incapable of rearrangement under large strain. The bottom layer of graphene film on the substrate is likely to fracture randomly under stretching. The upper layer of graphene film which conformally wrapped on the AgNWs should break around the AgNWs to accommodate the deformation due to local perturbation. That is, the upper and bottom layers of graphene films have high possibility to be torn apart relatively at different positions. The graphene fragments can bridge the AgNWs and keep the continuity of GAG films. As a result, the AgNW networks show electrical failure whereas the GAG films are tolerable to cyclic tests at large strain without significant conductivity change.

The application potential of the GAG films is demonstrated as efficient stretchable transparent EMI shielding devices. The total EMI shielding effectiveness (SE_T) of the GAG films are plotted as a function of electromagnetic wave frequency in Fig. 3a. The EMI SE_T decreases as the GAG film transmittance increasing. At the transmittance of 62, 71, 80 and 88%, the average EMI SE_T in the frequency range of 8.2 – 12.4 GHz (X-band) is 58, 49, 41 and 36 dB, respectively. These results demonstrate that the EMI SE_T of the GAG films can be easily controlled by adjusting the AgNW areal densities. The EMI SE_T also remains almost stable under stretching strain smaller than 30% and decreases by 13% at 40% strain, which corresponds well with the slight variation trend of sheet resistance upon stretching. Even if the applied strain is 50%, the EMI SE_T is higher than 27 dB, indicating that more than 99% of the incident electromagnetic waves are shielded. The good EMI shielding performance together with the high transparency and stretchability place the GAG films among the most promising EMI shielding materials, especially for uses of smart windows and deformable displays.

The EMI shielding performance of the GAG films is compared with AgNW networks in the aspects of EMI SE_R and SE_A (SE by reflection and absorption). At the same transmittance of 88%, the average SE_R (SE_A) of the AgNW networks and the GAG films is 5 (16) and 9 (27) dB, respectively (Fig. 3b). This phenomenon can be understood by analyzing the ε' and ε'' (real part and imaginary part of permittivity). As the ε' *versus* ε'' curves illustrated in Fig. 3c, both ε' and ε'' of the GAG films are higher than the AgNW networks, which is attributed to the higher electrical conductivity of the former according to the free electron theory and effective medium theory. In addition, based on Debye theory and deep deduction, the ε'-ε'' curve of an ideal EMI shielding material behaves like a semicircle, defining as Cole-Cole semicircle [29]. Each semicircle represents a kind of Debye dipolar relaxation process. There is only one Cole-Cole semicircle for the AgNW networks. More than two are observed for the GAG films, suggesting multiple superimposed dielectric polarization processes for the incident electromagnetic waves. These results are likely to occur due to the following factors (insets in Fig. 3c). First, many electrons may be localized near the AgNWs

junctions under the action of alternating electromagnetic waves due to the small nanometre-gap between adjacent AgNWs, which yields dielectric polarization. This analysis is supported by the results showing that the AgNW junctions can be welded by the Joule heat generated during microwave irradiation process [30]. Second, the defects such as vacancies and wrinkles in graphene, as evidenced by our Raman spectrum, play the role of permanent dipoles and thereby providing another type of integral dielectric polarization. Third, taking the resistivity difference between AgNWs and graphene into account, interfacial polarization may be involved in the high permittivity of the GAG films.

The EMI shielding mechanism of GAG films is described (Fig. 3d) in the aspects of EMI SE_R and SE_A, respectively. The high EMI SE_R mainly consists of three reflection processes. The first reflection happens at the surface of upper layer graphene whose impedance does not match with the free space impedance. Another reflection occurs when the external radiation field encounters the AgNWs and most of electromagnetic waves will be immediately reflected backward by the AgNWs. The electromagnetic waves that pass through the AgNWs will be reflected by the bottom graphene. Furthermore, two layers of graphene can form a cavity that reflect the electromagnetic waves back and forth until they are consumed. On the other hand, the absorption mechanism also contributes the electromagnetic wave attenuation. First, both the conduction loss and multiple polarization processes provided by the graphene films dominate the high EMI SE_A. Second, the AgNWs in the GAG film form intricate percolation network that can induce high electromagnetic wave absorption. In details, the average diameter of AgNWs is more than four magnitudes lower than the wavelength of microwaves, and thus the AgNWs can be treated as conducting filaments and the reticulated networks can be viewed as many resistance–inductance–capacitance (RLC) coupled circuits for the electromagnetic waves. In this case, the electromagnetic field could induce current on the RLC circuits that rapidly be attenuated within the resistive network in the form of Joule heat. Compared with the AgNW networks, the resistivity of AgNWs is reduced by the graphene cladding process, which decreases the junction barrier for electron transport within the RLC resonance circuits, thereby inducing enhanced electromagnetic wave absorption. The above absorption mechanisms coincide with the high dielectric tangent loss ($\tan \delta_E = \varepsilon''/\varepsilon'$) of the GAG films, verifying their good capability to convert electrical energy into heat. Therefore, the GAG films with better interconnection than AgNW networks should more efficiently reflect and absorb the electromagnetic waves with smooth frequency selectivity.

Conclusions

In summary, we have developed a GAG film for stretchable transparent conductors. The optoelectronic properties of the GAG films are shown to be tunable through adjusting the areal density of AgNWs. The graphene films can enhance the stretchability and EMI SE of AgNW networks by providing the AgNW backbone with extra electron transport paths and offering dielectric polarization and multiple reflection processes for the attenuation of incident electromagnetic waves. The GAG film with an average transmittance of 88% maintain an EMI SE of 31 dB after repeated stretching and release at 40% strain.

This work therefore demonstrates an efficient strategy to improve the total performance of AgNW networks. The GAG films have application potential in wearable optoelectronic and EMI shielding devices.

Declarations

Acknowledgment

The work is supported by the National Natural Science Foundation of China (No. 51902049), the Fund from Jilin Province (No. 20200201076JC).

Conflict of interest

The authors declare that they have no conflict of interest.

References

[1] Kim K, Park YG, Hyun BG, Choi M, Park JU (2019) Recent advances in transparent electronics with stretchable forms. Adv. Mater. 31:1804690.

[2] Xue R, Wang X, Chen X, Zhang M, Qi S (2016) Transparent stretchable composite conductor based on silver nanowires with hybrid structure. J. Mater. Sci. 51:7211–7219.

[3] Han Y, Liu Y, Han L, Lin J, Jin P (2017) High-performance hierarchical graphene/metal-mesh film for optically transparent electromagnetic interference shielding. Carbon 115:34–42.

[4] Dong H, Wu Z, Jiang Y, Liu W, Li X, Jiao B, Abbas W, Hou X (2016) A flexible and thin graphene/silver nanowires/polymer hybrid transparent electrode for optoelectronic devices. ACS Appl. Mater. Interfaces 8:31212–31221.

[5] Zheng B, Zhu Q, Zhao Y (2019) Flexible silver nanowire transparent conductive films prepared by an electrostatic adsorption self-assembly process. J. Mater. Sci. 54:5802–5812.

[6] Zhang B, Li W, Nogi M, Chen C, Yang Y, Sugahara T, Koga H, Suganuma K (2019) Alloying and embedding of Cu-Core/Ag-shell nanowires for ultrastable stretchable and transparent electrodes. ACS Appl. Mater. Interfaces 11:18540–18547.

[7] Hong S, Lee H, Lee J, Kwon J, Han S, Suh YD, Cho H, Shin J, Yeo J, Ko SH (2015) Highly stretchable and transparent metal nanowire heater for wearable electronics applications. Adv. Mater. 27:4744.

[8] Li P, Ma JG, Xu HY, Lin D, Xue XD, Yan XZ, Xia P, Liu YC (2016) Flexible transparent heaters based on silver nanotrough meshes. J. Alloys Compd. 664:764.

[9] Sohn H, Woo YS, Shin W, Yun D-J, Lee T, Kim FS, Hwang J (2017) Novel transparent conductor with enhanced conductivity: hybrid of silver nanowires and dual-doped graphene. Appl. Surf. Sci. 419:63—69.

[10] Kim KS, Zhao Y, Jang H, Lee SY, Kim JM, Kim KS, Ahn J-H, Kim P, Choi J-Y, Hong BH (2009) Large-scale pattern growth of graphene films for stretchable transparent electrodes. Nature 457:706—710.

[11] Li P, Ma JG, Xu HY, Zhu HC, Liu YC (2017) The role of graphene in electrical heating and mechanical performances of aligned silver nanowires–graphene hybrid transparent heaters. Appl. Phys. Lett. 110:161901.

[12] Miao J, Chen S, Liu H, Zhang X (2018) Low-temperature nanowelding ultrathin silver nanowire sandwiched between polydopamine-functionalized graphene and conjugated polymer for highly stable and flexible transparent electrodes. Chem. Eng. J. 345:260—270.

[13] Kim DG, Choi JH, Choi D-K, Kim SW (2018) Highly bendable and durable transparent electromagnetic interference shielding film prepared by wet sintering of silver nanowires. ACS Appl. Mater. Interfaces 10:29730—29740.

[14] Lee D, Lee H, Ahn Y, Lee Y (2015) High-performance flexible transparent conductive film based on graphene/AgNW/graphene sandwich structure. Carbon 81:439—446.

[15] Seo TH, Kim BK, Shin G, Lee C, Kim MJ, Kim H, Suh E-K (2013) Graphene-silver nanowire hybrid structure as a transparent and current spreading electrode in ultraviolet light emitting diodes. Appl. Phys. Lett. 103:051105.

[16] Deng B, Hsu P-C, Chen G, Chandrashekar BN, Liao L, Ayitimuda Z, Wu J, Guo Y, Lin L, Zhou Y, Aisijiang M, Xie Q, Cui Y, Liu Z, Peng H (2015) Roll-to-roll encapsulation of metal nanowires between graphene and plastic substrate for high-performance flexible transparent electrodes. Nano Lett. 15:4206—4213.

[17] Zhu X, Xu J, Qin F, Yan Z, Guo A, Kan C (2020) Highly efficient and stable transparent electromagnetic interference shielding films based on silver nanowires. Nanoscale 12:14589—14597.

[18] Chae WH, Sannicolo T, Grossman JC (2020) Double-sided graphene oxide encapsulated silver nanowire transparent electrode with improved chemical and electrical stability. ACS Appl. Mater. Interfaces 12:17909—17920.

[19] Park J, Kim J, Kim K, Kim S-Y, Cheong WH, Park K, Song JH, Namgoong G, Kim JJ, Heo J, Bien F, Park J-U (2016) Wearable, wireless gas sensors using highly stretchable and transparent structures of nanowires and graphene. Nanoscale 8:10591—10597.

[20] Choi TY, Hwang B-U, Kim B-Y, Trung TQ, Nam YH, Kim D-N, Eom K, Lee N-E (2017) Stretchable, transparent, and stretch-unresponsive capacitive touch sensor array with selectively patterned silver nanowires/reduced graphene oxide electrodes. ACS Appl. Mater. Interfaces 9:18022—18030.

[21] Yang S-B, Choi H, Lee DS, Choi C-G, Choi S-Y, Kim I-D (2015) Improved optical sintering efficiency at the contacts of silver nanowires encapsulated by a graphene layer. Small 11:1293—1300.

[22] Yang Y, Chen S, Li W, Li P, Ma J, Li B, Zhao X, Ju Z, Chang H, Xiao L, Xu H, Liu Y (2020) Reduced graphene oxide conformally wrapped silver nanowire networks for flexible transparent heating and electromagnetic interference shielding. ACS Nano 14:8754—8765.

[23] Kumar P, Shahzad F, Hong SM, Koo CM (2016) A flexible sandwich graphene/silver nanowires/graphene thin film for high-performance electromagnetic interference shielding. RSC Adv. 6:101283—101287.

[24] Liu B-T, Kuo H-L (2013) Graphene/silver nanowire sandwich structures for transparent conductive films. Carbon 63:390—396.

[25] Liang J, Li L, Tong K, Ren Z, Hu W, Niu X, Chen Y, Pei Q (2014) Silver nanowire percolation network soldered with graphene oxide at room temperature and its application for fully stretchable polymer light-emitting diodes. ACS Nano 8:1590—1600.

[26] Chen R, Das SR, Jeong C, Khan MR, Janes DB, Alam MA (2013) Co-percolating graphene-wrapped silver nanowire network for high performance, highly stable, transparent conducting electrodes. Adv. Funct. Mater. 23:5150—5158.

[27] Li P, Zhang W, Ma J, Wang X, Xu H, Cong L, Liu Y (2018) Solution-grown serpentine silver nanofiber meshes for stretchable transparent conductors. Adv. Electron. Mater. 4:1800346.

[28] Li P, Wang X, Ma J, Wang T, Zhang W, Xu H, Liu Y (2019) Interface engineering of solution-grown silver nanofiber networks designed as flexible transparent electrodes. J. Mater. Chem. C 7:3924—3933.

[29] Wu S, Zou M, Li Z, Chen D, Zhang H, Yuan Y, Pei Y, Cao A (2018) Robust and stable Cu nanowire@graphene core–shell aerogels for ultraeffective electromagnetic interference shielding. Small 14:1800634.

[30] Jung PH, Kim YD, Sung YH, Lee H (2017) Microwave welding of silver nanowires for highly transparent conductive electrodes. Phys. Status Solidi A 214:160098.

Figures

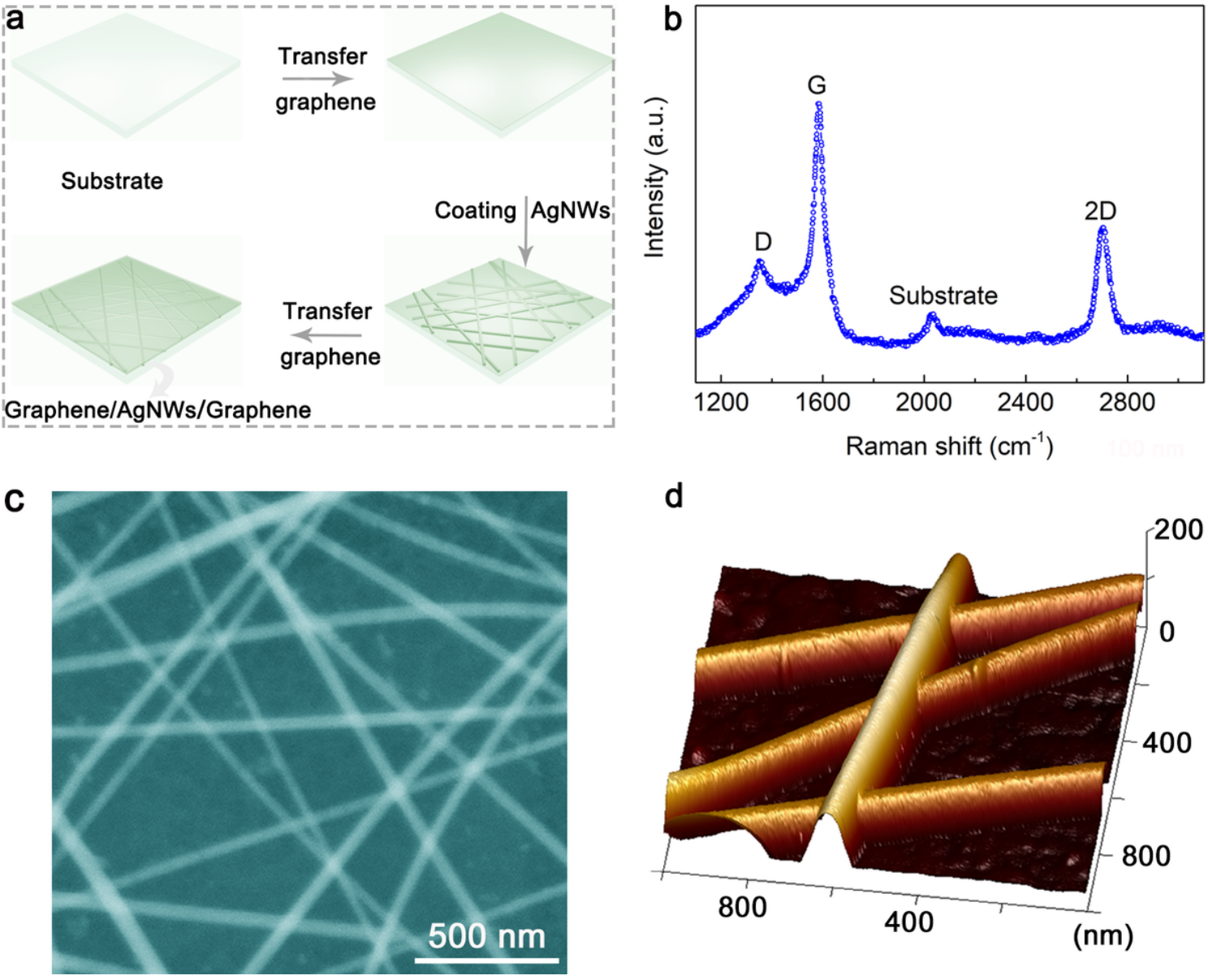

Figure 1

(a) Schematic diagram of the preparation process for the GAG film. (b–d) Raman spectrum and SEM and AFM images of the GAG film.

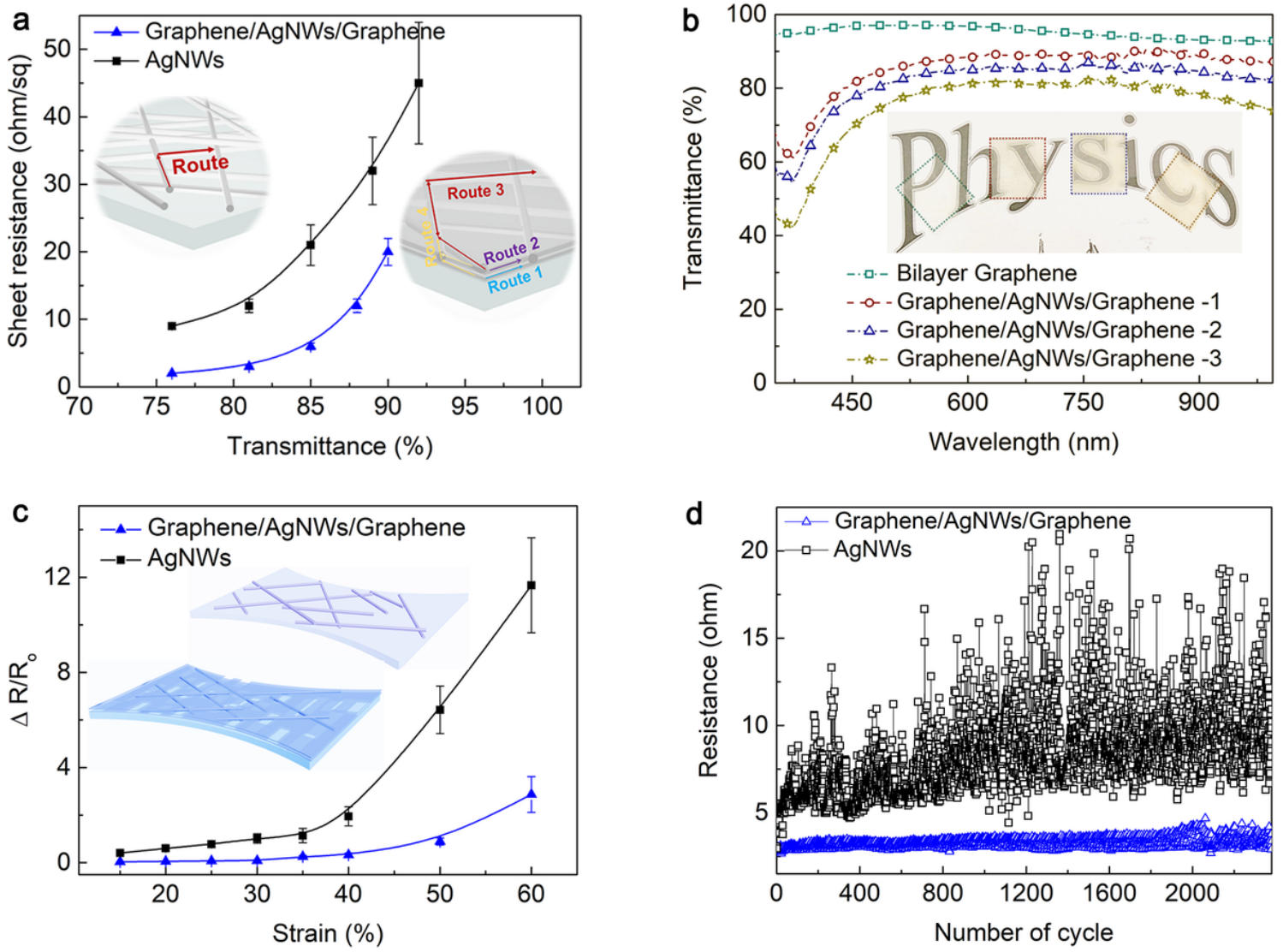

Figure 2

(a) Sheet resistance versus transmittance at 550 nm for the GAG films and the AgNW networks. Insets are the schematic diagram showing the conducting paths. (b) Transmission spectra and corresponding photograph (inset) of bilayer graphene and GAG films. Resistance as a function of strain (c) and the number of stretching cycles (d) for the GAG film and the AgNW network. Insets in (c) are the schematic diagrams showing the stretched samples.

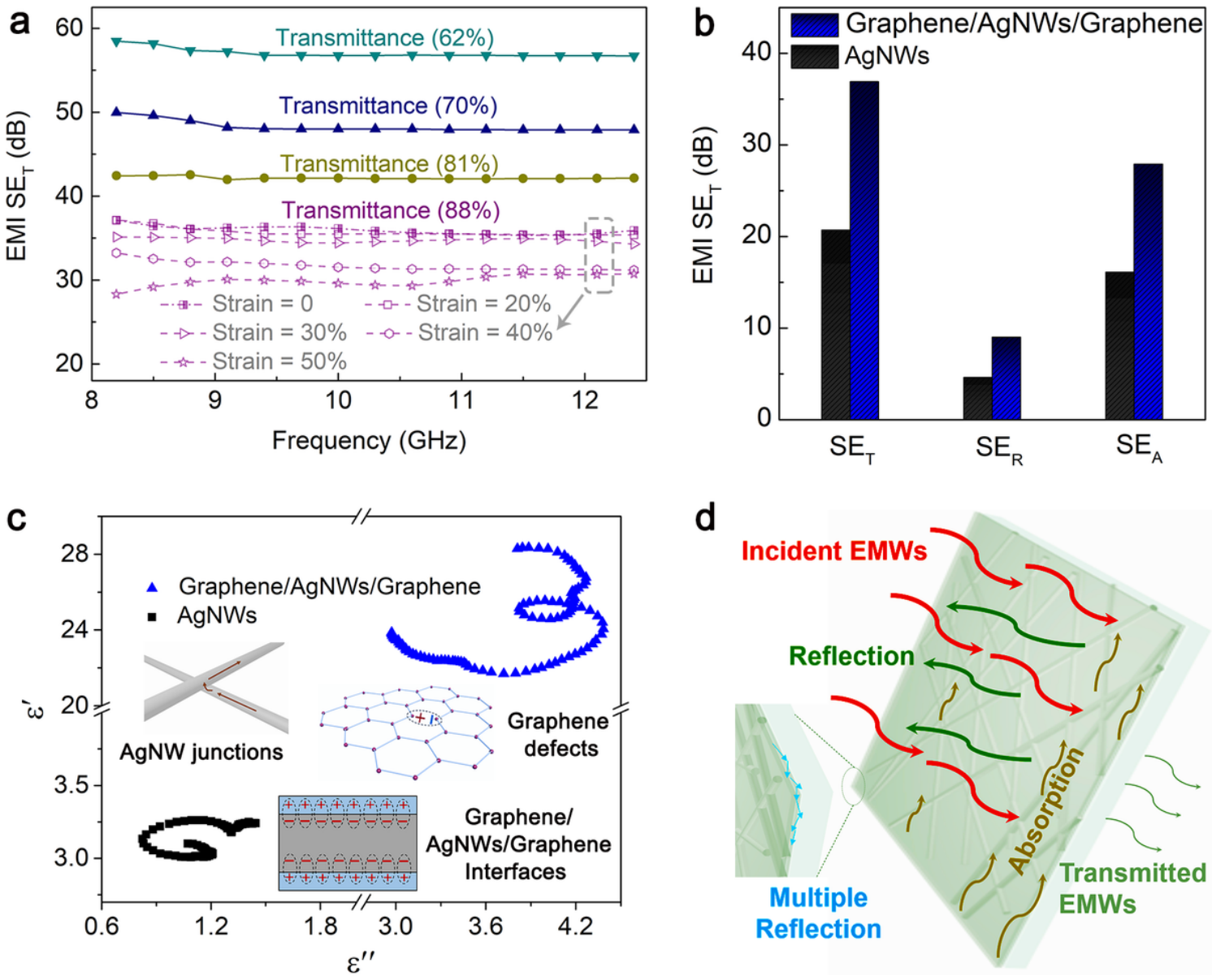

Figure 3

(a) EMI SET in X-band of the graphene/AgNWs/graphene (GAG) films with transmittance of 62, 70, 81 and 88%, and the GAG film (at 88%) after applied strains of 0–50%. (b) Average EMI SET, SEA and SET values and (c) ε' versus ε" curves for the GAG film and AgNW network in X-band. Insets are the schematic diagram of various dielectric polarization processes. (d) Schematic diagram showing the EMI shielding mechanism of the GAG films.